

Article

Pressure-Induced Neutral to Ionic Phase Transition in TTF-Fluoranil, DimethylTTF-Fluoranil and DimethylTTF-Chloranil: A Comparative THz Raman Study

Elena Ferrari ^{1,2} , Francesco Mezzadri ¹  and Matteo Masino ^{1,*} 

¹ Dipartimento di Scienze Chimiche, Della Vita e Della Sostenibilità Ambientale & INSTM-UdR Parma, Parco Area delle Scienze, 17/A, 43124 Parma, Italy; elena.ferrari@imem.cnr.it (E.F.)

² IMEM-CNR, Parco Area delle Scienze 37/A, 43124 Parma, Italy

* Correspondence: matteo.masino@unipr.it

Abstract: The Neutral to Ionic phase Transition (NIT) that occurs in few mixed stack charge transfer cocrystals at high pressure or low temperature is a charge instability combined with a structural instability. The lattice contraction, which increases the 3D Coulomb interactions, favors a higher degree of charge transfer. Due to Peierls instability, this leads to the dimerization of the stack, breaking its inversion symmetry. The 3D interactions also determine the arrangement of the adjacent dimerized polar stacks, making the ionic phase ferroelectric or antiferroelectric. The role of these parameters that modulate the NIT has been widely studied in Tetrathiafulvalene-haloquinone cocrystals. Here, we compare the high-pressure behavior of three of them: the newly synthesized TTF-FA and DM-TTF-FA with the known DM-TTF-CA and isostructural DM-TTF-FA. We followed the evolution of the lattice phonons via THz Raman spectroscopy, assessing the pressure-dependent structural changes. While the FA-based crystals undergo strong first-order NIT, DM-TTF-CA shows a continuous transition. The high-pressure behavior of each crystal is also compared with the low-temperature behavior.

Keywords: CT crystals; phase transition; lattice phonons



Citation: Ferrari, E.; Mezzadri, F.; Masino, M. Pressure-Induced Neutral to Ionic Phase Transition in TTF-Fluoranil, DimethylTTF-Fluoranil and DimethylTTF-Chloranil: A Comparative THz Raman Study. *Crystals* **2023**, *13*, 1428. <https://doi.org/10.3390/cryst13101428>

Academic Editor: Younes Hanifehpour

Received: 7 September 2023

Revised: 20 September 2023

Accepted: 22 September 2023

Published: 26 September 2023



Copyright: © 2023 by the authors. Licensee MDPI, Basel, Switzerland. This article is an open access article distributed under the terms and conditions of the Creative Commons Attribution (CC BY) license (<https://creativecommons.org/licenses/by/4.0/>).

1. Introduction

Few mixed-stack organic charge transfer (CT) cocrystals display a peculiar instability known as the Neutral to Ionic phase Transition (NIT). These materials are based on π -electron donor and acceptor molecules alternating along 1D stacks. Such an arrangement favors the overlap between the frontier molecular orbitals and the CT interaction between them. This results in a partial ionization of the molecules: based on the ionicity ρ , CT crystals are classified as neutral (N) if $\rho < 0.5$ or ionic (I) otherwise [1].

The transition occurs at high pressure or low temperature, as the resulting lattice contraction increases the 3D Coulomb interactions, eventually leading the system from a N ground state to an I one [2–4]. Since I regular stacks are subject to Peierls instability, the ionicity increase is always accompanied by the stack dimerization. Thus, the NIT involves the interplay between two instabilities of different origin: a charge one, due to 3D Coulomb interactions, and a structural one, due to electron–phonon coupling. While the former favors a discontinuous ionicity increase, the latter drives the stack to continuous symmetry breakage [5–7]. Depending on the relative strength of these microscopic parameters, the NIT can be first- or second-order.

The 3D interactions also influence the arrangement of the adjacent dimerized polar stacks. While the prototypical system Tetrathiafulvalene-Chloranil (TTF-CA) is ferroelectric, other close materials as DimethylTTF-CA (DM-TTF-CA) are antiferroelectric.

In this context, THz Raman spectroscopy, which probes the lattice phonons, is a powerful tool for detecting changes in the crystal packing, i.e., lattice symmetry, the number of molecules in the unit cell, and the structural order. This is very useful when the

structural data can be difficult to measure, as under pressure, inside the Diamond Anvil Cell. Here, we compare the pressure-induced NIT in three TTF-haloquinone-based charge transfer cocrystals: the newly synthesized TTF-Fluoranil (TTF-FA) [8] and DimethylTTF-FA (DMTTF-FA) with the known DMTTF-CA [9,10], isostructural with DMTTF-FA. While the FA-based crystals undergo strong first-order NIT, DMTTF-CA shows continuous behavior. In all the crystals, the stack dimerization is coupled with the doubling of the unit cell, leading to an antiferroelectric state.

2. Materials and Methods

2.1. Crystal Growth

TTF-FA and DMTTF-FA crystals were grown by rapidly evaporating saturated toluene solutions of the two precursors, as described in [8]. This growth method is required to avoid side reactions during the synthesis. DMTTF-CA crystals were instead grown by sublimation, as described in Ref. [9]. DMTTF was purified by recrystallization from toluene before use. Microscopic images of the crystals are shown in Figures S1–S3.

2.2. Spectroscopic Measurements

The Raman spectra were measured with a Horiba LabRAM HR Evolution Raman microspectrometer using a 633 nm laser coupled with a ULF Bragg filter or a 785 nm laser coupled with an edge filter. The laser power was kept below 0.1 mW to avoid sample heating. The measurements were performed on oriented single crystals with parallel configuration of polarization: both the exciting and the scattered light were polarized parallel or perpendicular to the stack direction of the three crystals. For TTF-FA and DMTTF-CA, the crystal faces were indexed by XRD, while for DMTTF-FA only the stack direction *a* was identified due to the presence of the CT excitation in the IR spectra polarized along the stack.

For the high-pressure measurements, the samples were placed in a diamond anvil cell (DAC) using a brass gasket to allow finer pressure tuning in the range 0.1–2 GPa. The hole containing the sample was filled with Nujol oil, which was used as a pressure transmitting medium. The DAC was fitted under both IR and Raman microscopes. For Raman, a 20× magnification objective was used, as its working distance was suitable for focusing the laser beam on the sample inside the cell. The pressure was measured according to the ruby fluorescence method [11]. To increase the wavelength accuracy, the spectrum of a Ne calibration lamp was acquired together with the ruby fluorescence without moving the grating (pressure error 0.05 GPa). Measurements performed on rubies located in different positions of the hole confirmed the pressure homogeneity.

2.3. Single-Crystal X-ray Diffraction

The DMTTF-FA and DMTTF-CA crystal structures were determined via single-crystal X-ray diffraction using a Bruker D8 Venture diffractometer (MoK α radiation $\lambda = 1.54178$ Å). Data collections were carried out at 150 K in order to limit the atoms displacements, thus simplifying the refinement of the disordered molecular moieties. Intensities integration was carried out using the SADABS program for DMTTF-CA, while due to twinning detected in all the checked crystals, integration for DMTTF-FA required the TWINABS software. Absorption correction was applied using a multi-scan model. All the integration and correction processes were carried out using the APEX3 suite [12]. The structure solution was carried out with the SHELXT program and refined full-matrix using SHELXL [13]. All non-hydrogen atoms of DMTTF-CA were refined with anisotropic atomic displacement parameters (ADP), while the hydrogen atoms were refined with a riding model on the corresponding parent atoms. Due to the presence of disorder involving about 10% of the molecules, constraints were used to model the geometry of the disordered moieties and isotropic ADPs were used. On the contrary, the molecules with 0.9 occupancy were refined with anisotropic ADPs, with riding hydrogen atoms.

3. Results

3.1. Structure Comparison

Before discussing the high-pressure behavior of the three materials, it is convenient to compare the starting crystal structures in ambient conditions. The crystal structures of TTF-FA and DMTTF-CA are already known [8,9,14], while that of DMTTF-FA was reported for the first time. We have, however, collected the diffraction data of DMTTF-CA to compare the possible disorder features of the crystals obtained using the present crystallization method. The three crystal structures share many common features: the same $P - 1$ space group, a single DA pair in the unit cell, and a mixed regular stack motif, with the molecules located on the inversion centers (Figure 1 and Table 1).

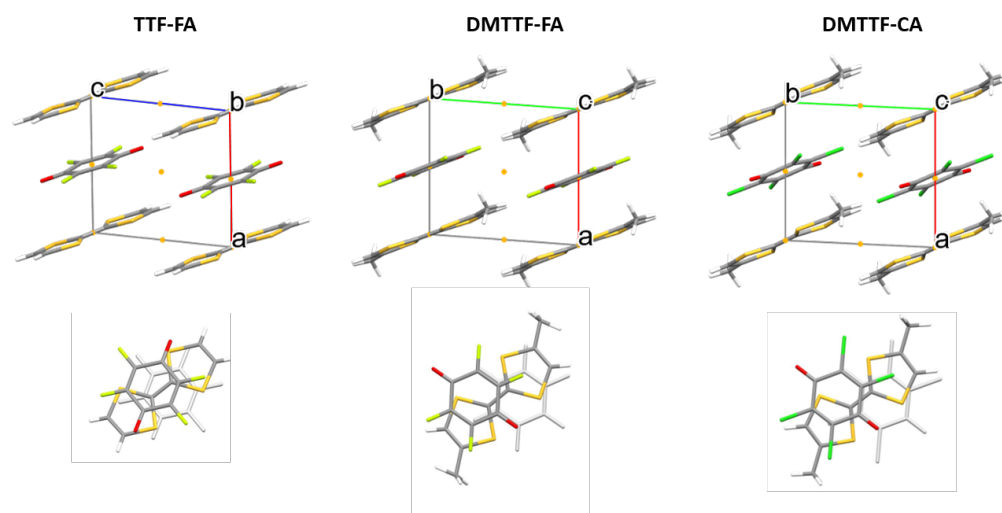


Figure 1. Comparison between the unit cells and DA overlaps in TTF-FA, DMTTF-FA and DMTTF-CA.

Table 1. Comparison between the structural parameters of TTF-FA, DMTTF-FA, and DMTTF-CA.

	TTF-FA	DMTTF-FA	DMTTF-CA
Space group	$P - 1$	$P - 1$	$P - 1$
a (Å) \AA	7.054 ¹	6.9278 ¹	7.1903 ¹
b (Å)	7.304	7.6275	7.6250
c (Å)	7.359	7.6919	8.4799
α (deg)	106.15	97.581	96.162
β (deg)	93.101	97.447	103.779
γ (deg)	102.419	93.074	91.137
V (Å ³)	353.037	398.467	448.434
Z	1	1	1
d_{DA} / Å	3.365	3.234	3.345
t (eV) ²	0.32	0.32	0.21

¹ Stack direction; ² Charge transfer integrals calculated according to the methods described in Ref. [15].

The crystal structure of DMTTF-CA determined for the present work confirms the previous determination, with the absence of any detected disorder, while in DMTTF-FA all the molecules have a 10% probability of being slightly rotated with respect to the equilibrium position of the ordered structure. Such disorder is more likely due to the presence of a residual fraction of *cis* DMTTF molecules, which can arrange themselves differently in the lattice. Another possible explanation for the disorder is a random arrangement of the DMTTF molecules in the crystal lattice. Due to the 2,5 substitution, DMTTF has two equivalent orientations, which are related by a rotation of 180° around the long molecular axis. Also, the very rapid crystal growth might favor this kind of disorder.

DMTTF-FA is isomorphous with DMTTF-CA, but the latter has larger lattice parameters due to its bulkier CA acceptor. The main difference is along the c direction. The

interchain interaction pattern and the DA overlap are the same for the two crystals. In both crystals, the quinone O-O axis is nearly perpendicular to the long TTF axis, which differs from TTF-FA (Figure 1).

3.2. Pressure-Induced Transition

3.2.1. TTF-FA

TTF-FA undergoes a first-order phase transition around 0.5 GPa, which is associated with a colour change from green to brown (Figure S1a,b) and an increase in ionicity from $\rho = 0.15$ at ambient pressure to $\rho = 0.7$ around 1 GPa (Figure S4). The transition is reversible but the crystals crack as the transition is cycled (Figure S1c). During the transition, the optical axes are always unchanged. Although the hysteresis is below the pressure accuracy, the coexistence of both phases sometimes occurs near the critical pressure point, suggesting the presence of metastable phases. The phenomena associated with the pressure-induced transition are very similar to the low-temperature behavior described in our previous work [8].

A deeper insight into the associated structural changes can be obtained directly via Raman observation of the lattice phonons, in the THz range. These modes are strongly affected by the intermolecular interactions and thus reflect the crystal packing. The number of phonon bands and their symmetry species gives information both on the symmetry and on the number of molecules in the unit cell.

The sudden appearance of many phonon bands in the THz Raman spectra demonstrates the doubling of the unit cell (Figure 2a). Their pattern and relative intensities correspond to the low-temperature spectra (Figure 2b). The different bandwidth is only a thermal effect, as the high-pressure measurements are performed at room temperature. The slight frequency hardening observed at 0.9 GPa is due to the fact that the lattice contraction at high pressure is larger than that at low temperature. This makes us confident that the high-pressure structure is the same as the low-temperature one [8].

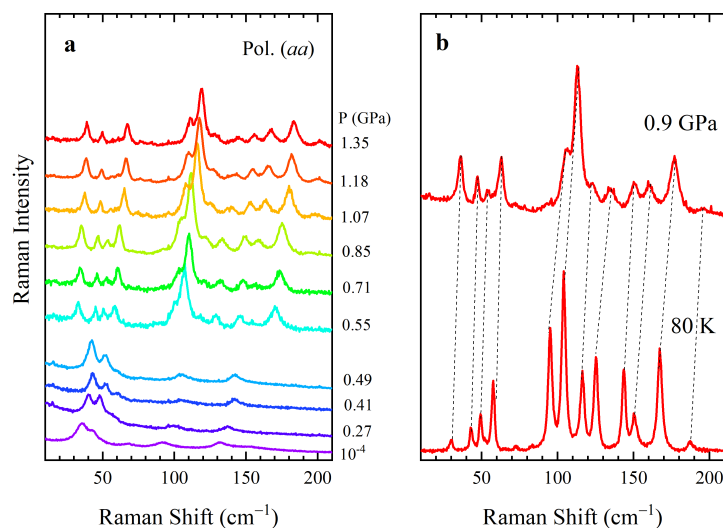


Figure 2. (a) Pressure-dependent low-frequency Raman spectra of TTF-FA, measured with both the exciting and scattered light polarized parallel to the stack. (b) Comparison between the low-frequency Raman spectra of TTF-FA at $p = 0.9$ GPa and room temperature (upper panel) and at ambient pressure and $T = 80$ K (lower panel). $\lambda_{exc} = 633$ nm.

The stack dimerization at high pressure is highlighted by the simultaneous IR activation of the totally symmetric intramolecular modes, which are polarized along the stack (Figure S4). Also, the IR spectra are very similar to the corresponding low-temperature ones [8].

In each phase, the evolution of the spectra is strongly discontinuous and never anticipates the corresponding spectra of the other phase approaching the transition. The phonon bands display the typical linear frequency hardening with increasing pressure.

The spectra maintain the same polarization throughout the transition, even when cycling occurs. The correspondence between the optical axes of the two phases demonstrates that the transition mechanism is concerted.

In conclusion, there is clear evidence that the high-pressure and low-temperature phases are the same ionic phase, with a doubled unit cell containing two dimerized stacks with antiferroelectric arrangement. Also, the transition mechanism is probably the same for both conditions.

3.2.2. DMTTF-FA

At ambient pressure, DMTTF-FA is in the neutral state, with $\rho = 0.14$, according to the frequency shifts of the FA charge-sensitive vibrations (Figure S5). At 0.5 GPa, a first-order phase transition occurs with a color change from green to brown (see Figure S2a,b). At the same time the ionicity jumps to $\rho = 0.45$.

The transition is reversible without any detectable hysteresis, but with crystal damage. Many parallel cracks appear if the process is cycled (Figure S2c). Unlike TTF-FA, no transition occurs at low temperature, despite the identical critical pressure and the similar parameters of the two systems.

At ambient pressure, DMTTF-FA THz Raman spectra display five broad and overlapping phonon bands (Figure 3b), which separate into six different ones at low temperature (Figure S7). The number of phonon bands is consistent with the predictions based on the triclinic unit cell containing $Z = 1$ pairs: only the six librations are Raman active. Also, the large phonon bandwidth agrees with the structural disorder identified via XRD.

The transition occurring above 0.5 GPa is associated with the appearance of many new bands and the intensity enhancement of the spectra measured with both exciting and scattered light polarized along the stack (Figure 3a). These bands may be assigned to translational phonons, which are activated by the inversion symmetry breaking along the stack and their high Raman intensity might be related to a pre-resonance effect with the CT excitation polarized in the same direction.

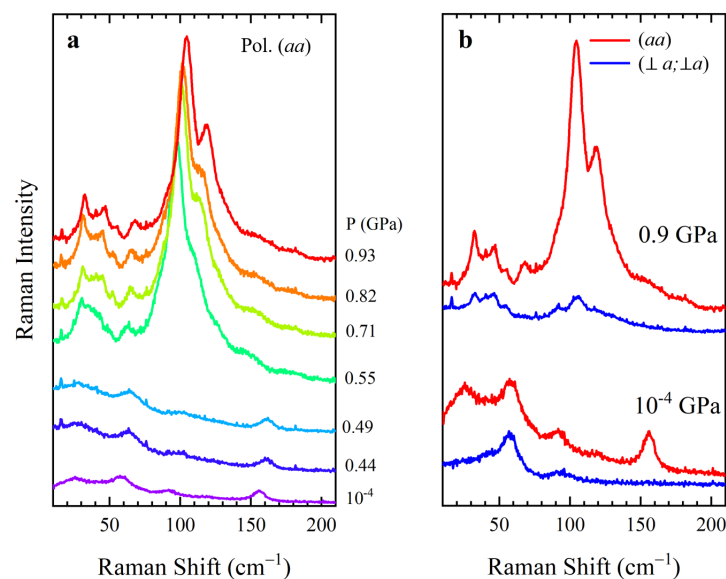


Figure 3. (a) Pressure-dependent low-frequency Raman spectra of DMTTF-FA, measured with both the exciting and scattered light polarized parallel to the stack. $\lambda_{exc} = 633$ nm (b) Polarized low-frequency Raman spectra of DMTTF-FA at atmospheric pressure (10^{-4} Pa) and 0.9 GPa, measured with both the exciting and scattered light polarized parallel or perpendicular (blue lines) to the stack. The spectra measured at atmospheric pressure were multiplied by 3 for clarity. $\lambda_{exc} = 633$ nm.

At high pressure, eight phonon bands can be resolved, but more weaker bands might be present. The exact number is uncertain due to the superimposition of broad bands. The phonon bands are much broader in DMTTF-FA than in TTF-FA at similar pressures (Figure S8). This means that the DMTTF-FA structural disorder is maintained in the high pressure brown phase. Regardless, the number of bands demonstrates the unit cell doubling in the brown phase.

In DMTTF-FA, the stack also dimerizes at the transition: the IR spectra polarized along the stack direction are suddenly saturated by strong bands, corresponding to the DMTTF and FA totally symmetric modes (Figure S5). Thus, the DMTTF-FA high-pressure structure is likely characterized by the antiferroelectric arrangement of adjacent dimerized stacks.

3.2.3. DMTTF-CA

DMTTF-CA is known to display second-order valence instability induced by pressure or temperature [9,16–18]. A recent investigation found the high-pressure phase to be different from the low-temperature one [19]. In both phases, the unit cell is doubled and the dimerized stacks are arranged antiferroelectrically. The cell doubling occurs along the *c* axis at low temperature and along the *b* axis at high pressure. Both transitions are continuous, possibly involving an intermediate disordered phase [9,19].

Furthermore, our previous work revealed anharmonic effects in the low-temperature THz Raman spectra, close to the transition [20]. Thus, the present high-pressure study aims to compare the pressure and temperature behavior of DMTTF-CA, as well as comparing DMTTF-CA with the two FA-based crystals.

At ambient pressure, the polarized low-frequency Raman spectra coincide with those reported in [10]. The investigated crystals lie on the *ab* plane and the exciting and scattered light were polarized parallel or perpendicular to the stack axis *a*.

As the pressure increases, the phonon bands blueshift with a linear trend and most of them are still present at 2 GPa. The *bb* polarized spectra, shown in Figure 4a, evolve in an unusual way. Around 0.8 GPa, a broad feature appears below 100 cm^{-1} , gains intensity up to 1 GPa, and finally disappears at 1.3 GPa. Such feature is present in this polarization only, suggesting an intermediate phase with low-dimensional disorder along the *b* direction. The cell doubling and the stack dimerization thus occur through a disordered phase, with lack of correlation along the *b* direction. All the pressure-dependent spectral changes are fully reversible and the spectra depend only on the applied pressure, not on the sample history. In the same pressure range, the charge-sensitive intramolecular vibrations shift towards lower frequencies, indicating an increase in ionicity (Figure S6), thus confirming that the structural changes and the ionicity increase occur at the same time.

This behavior, which is characterized by an intermediate disordered phase between 0.8 and 1.3 GPa, was not observed in the temperature-induced phase transition, followed with the same crystal orientation. Although a broad band also appeared at low temperature, it was visible only in the *aa* polarization in the ionic phase in close proximity to the critical temperature and was ascribed to the overtone of the dimerization soft mode [20]. Thus, the two phenomena must have different origins.

Above 1 GPa, new weak bands appear, signaling the symmetry breaking. While in the FA-based crystals, the transition results in an enhancement of the intensity of the *aa* polarized bands, this does not happen in DMTTF-CA, exciting at 633 nm (Figure 4b).

The new bands can be conveniently followed with 785 nm excitation (Figure 4c). Their intensity enhancement on moving the exciting wavelength toward the far-red is likely due to the pre-resonance with the CT transition, which is polarized along the stack direction *a*. Such intensity enhancement indeed occurs only when the exciting and scattered light are polarized along this direction (Figure 5). The low-frequency intramolecular modes of a_g symmetry coupled to the CT excitation are amplified as well.

Regardless, in all the crystals, the transition is associated with the appearance of new phonon bands, which are mainly active in polarization parallel to the stack. They can be sensibly assigned to translational phonons, which are coupled with the CT transition by

modulating the CT integrals between close D-A molecules. Such modes become Raman permissible when the stack dimerization breaks the inversion symmetry along the stack.

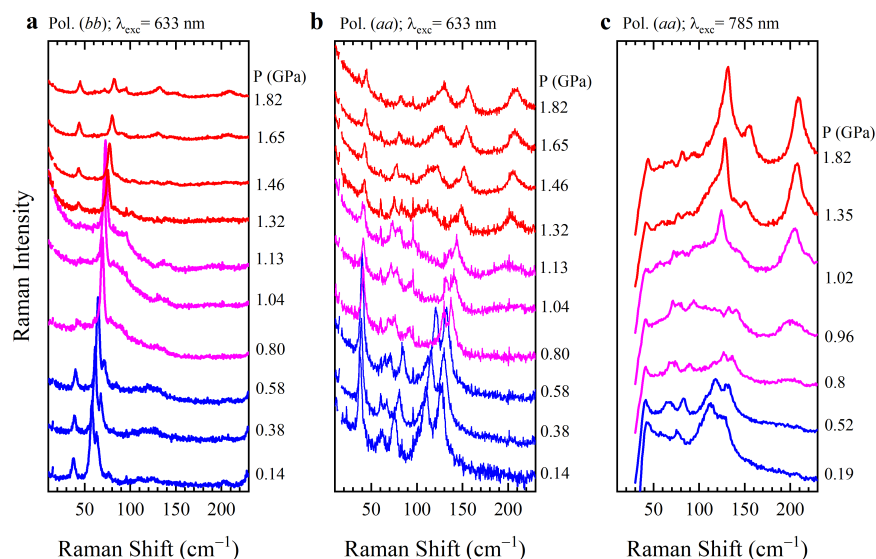


Figure 4. (a) Pressure-dependent low-frequency Raman spectra of DMTTF-CA, measured with both the exciting and scattered light polarized perpendicular to the stack. $\lambda_{exc} = 633$ nm (b,c) Pressure-dependent low-frequency Raman spectra of DMTTF-CA, measured with both the exciting and scattered light polarized parallel to the stack. $\lambda_{exc} = 633$ and 785 nm, respectively.

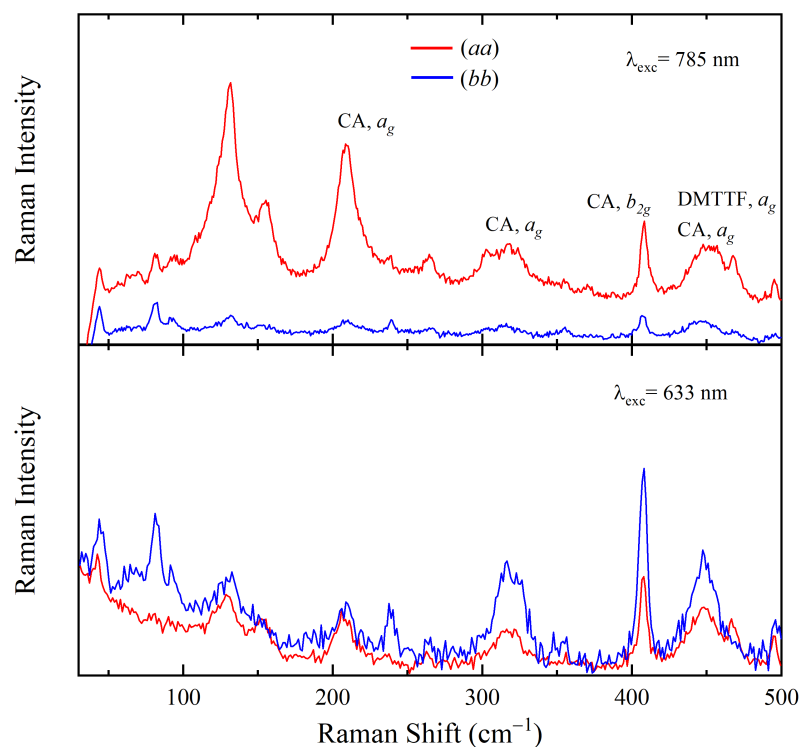


Figure 5. Raman spectra of DMTTF-CA at 1.82 GPa (ionic phase), measured with both the exciting and scattered light polarized parallel or perpendicular to the stack. $\lambda_{exc} = 785$ nm (upper panel) and 633 nm (lower panel). The $\lambda_{exc} = 785$ nm Raman spectra are completely dominated by the (aa)-polarization. The intramolecular band assignment is based on the comparison with the TTF-CA Raman spectra reported in Ref. [21]. Raman spectra measured with different laser excitation for the other system, TTF-FA and DMTTF-FA, are reported in Figures S9 and S10, respectively.

4. Discussion and Conclusions

We performed a detailed Raman study of the pressure-induced Neutral to Ionic phase Transition of three TTF-haloquinone cocrystals with close structures: TTF-FA, DMTTF-FA and DMTTF-CA. Furthermore, DMTTF-FA was grown and characterized for the first time.

It was determined that all three crystals undergo pressure-induced NIT: while the two FA based crystals show strongly discontinuous behavior, the DMTTF-CA transition is continuous and involves an intermediate disordered phase. The critical pressure, 0.5 GPa, is the same for the two FA-based crystals and is much lower than in DMTTF-CA (1.1 GPa). These features indicate the prevalence of Madelung energy over electron–phonon coupling in the case of the FA-based crystals, due to the smaller steric hindrance of the acceptor. On the contrary, electron–phonon coupling is the driving force in case of DMTTF-CA, where the Coulomb interactions between the chains are weakened due to the expanded crystal lattice, compared to the isomorphous DMTTF-FA structure [5–7].

The number and symmetry of the lattice phonon bands demonstrate that in all the crystals investigated, the transition involves the doubling of the unit cell, with an anti-ferroelectric arrangement of the adjacent dimerized stacks. In the case of TTF-FA, the coincidence between the high-pressure and low-temperature spectra indicates that the high-pressure phase is the same ionic phase obtained at low temperature and the transition mechanism is similar. On the contrary, the DMTTF-CA high-pressure phase is different with doubling of the unit cell along a different direction [19], as the phenomenology associated with the transition.

The absence of temperature-induced NIT in DMTTF-FA is unexpected. Kaźmierczak et al. reported that applying pressure between 0.2 and 0.5 GPa causes the same volume variation as cooling from 300 to 100 K [22]. This p-T correspondence is respected in the case of TTF-FA, whose transition occurs at a pressure of 0.5 GPa at 300 K or on cooling to 170 K at atmospheric pressure. Also, the isomorphous DMTTF-CA obeys the rule, with a critical pressure and critical temperature of 1.1 GPa and 65 K, respectively. Thus, the DMTTF-FA critical temperature would be expected above 65 K at atmospheric pressure.

A possible explanation for the DMTTF-FA discrepancy is that the neutral phase might be metastable at low temperature. This means that the transition is associated with a high activation barrier due to a significant structural rearrangement. Such a hypothesis is consistent with the extensive crystal cracking observed when the transition cycles (Figure S2c). Sample damage also occurred in the case of TTF-FA, whose transition is associated with a drastic rearrangement [8]. In the case of DMTTF-FA, the activation barrier might be either intrinsically higher than in TTF-FA or increased by the structural disorder. Another sensible explanation is that the different high-pressure and low-temperature behavior could be an intrinsic DMTTF-FA property, as in the case of DMTTF-CA.

The structural evolution of the three TTF-quinone systems was effectively probed via polarized THz Raman spectroscopy on oriented single crystals. Such an approach allowed us to probe the lattice phonon evolution and the occurrence of low-dimensional disorder along specific directions. We gained information about the symmetry of the unit cell and confirmed the crystallographic orientation relationship between the two phases through the transitions. This gives evidence that the transition mechanism is concerted and has a displacive nature. The Raman intensity of the phonon modes which drive the transition can be selectively amplified via pre-resonant enhancement with the CT excitation.

Supplementary Materials: The following supporting information can be downloaded at: <https://www.mdpi.com/article/10.3390/cryst13101428/s1>. Figure S1: TF-FA crystal inside the DAC, at (a) 0.2 and (b) 0.8 GPa. (c) Crystal cracking after cycling the transition; Figure S2: A DMTTF-FA crystal observed with polarized transmitted light, at (a) 0.2 and (b) 0.6 GPa. (c) Crystal cracking after the transition (red lines). The blue lines indicate the stack direction. The crystal on the right is twinned; Figure S3: A DMTTF-CA crystal, at (a) 0.5, (b) 0.7 and (c) 1.9 GPa. The elongation direction is the stack axis *c*; Figure S4: pressure dependent IR spectra of TTF-FA, measured on the *ab* plane with the light polarized perpendicular (left panel) or parallel to the stack (right panel). The ionicity ρ was estimated from the frequency shift of the FA charge sensitive modes [8]; Figure S5:

Pressure dependent IR spectra of DMTTF-FA, measured with the light polarized perpendicular (left panel) or parallel to the stack (right panel). The ionicity ρ was estimated from the frequency shift of the FA charge sensitive modes [8]; Figure S6: Pressure dependent extended Raman spectra of DMTTF-CA, measured with both the exciting and scattered light polarized perpendicular to the stack ($\lambda_{exc} = 633$ nm); Figure S7: Polarized low frequency Raman spectra of DMTTF-FA at 293 (upper panel) and 120 K (lower panel); Figure S8: Comparison between the low frequency Raman spectra of the high pressure phases of DMTTF-FA (upper panel) and TTF-FA (lower panel). The phonon bands are much broader in DMTTF-FA due to disorder; Figure S9: Raman spectra of TTF-FA at 0.9 GPa, measured with both the exciting and scattered light polarized parallel or perpendicular to the stack direction a. $\lambda_{exc} = 785$ nm (upper panel) and 633 nm (lower panel). The band assignment is based on the spectra of pure TTF and FA, reported in Refs [23,24]; Figure S10: Raman spectra of DMTTF-FA at 0.9 GPa, measured with both the exciting and scattered light polarized parallel or perpendicular to the stack. $\lambda_{exc} = 785$ nm (upper panel) and 633 nm (lower panel). The band assignment is based on the comparison with the TTF-FA spectra shown in Figure S9.

Author Contributions: E.F. prepared the crystal samples, performed IR and Raman spectroscopic measurements; E.F. and M.M. analyzed the spectroscopic data; F.M. performed X-Ray diffraction experiments and analyzed the data; E.F. and M.M. wrote the paper taking into consideration the input of all authors. M.M. conceived the work, planned experiments, and provided resources. The manuscript was written through contributions of all authors. All authors have read and agreed to the published version of the manuscript.

Funding: This research received no external funding.

Acknowledgments: Chiesi Farmaceutici SpA is acknowledged for the support with the D8 Venture X-ray equipment. This work has benefited from the equipment and framework of the COMP-HUB Initiative, funded by the 'Departments of Excellence' program of the Italian Ministry for Education, University and Research (MIUR, 2018–2022).

Conflicts of Interest: The authors declare no conflict of interest.

Sample Availability: Samples of the compounds are available from the authors.

Abbreviations

The following abbreviations are used in this manuscript:

CT Charge Transfer.
NIT Neutral to Ionic phase Transition.

References

1. Soos, Z.G. Theory of π -molecular charge-transfer crystals. *Annu. Rev. Phys. Chem.* **1974**, *25*, 121–153. [[CrossRef](#)]
2. Torrance, J.B.; Vazquez, J.E.; Mayerle, J.J.; Lee, V.Y. Discovery of a Neutral-to-Ionic Phase Transition in Organic Materials. *Phys. Rev. Lett.* **1981**, *46*, 253–257. [[CrossRef](#)]
3. Torrance, J.; Girlando, A.; Mayerle, J.; Crowley, J.; Lee, V.; Batail, P.; LaPlaca, S. Anomalous nature of neutral-to-ionic phase transition in tetrathiafulvalene-chloranil. *Phys. Rev. Lett.* **1981**, *47*, 1747–1750. [[CrossRef](#)]
4. Masino, M.; Castagnetti, N.; Girlando, A. Phenomenology of the Neutral-Ionic Valence Instability in Mixed Stack Charge-Transfer Crystals. *Crystals* **2017**, *7*, 108. [[CrossRef](#)]
5. Painelli, A.; Girlando, A. Zero-temperature phase diagram of mixed-stack charge-transfer crystals. *Phys. Rev. B* **1988**, *37*, 5748–5760. [[CrossRef](#)]
6. Girlando, A.; Painelli, A. Regular-dimerized stack and neutral-ionic interfaces in mixed-stack organic charge-transfer crystals. *Phys. Rev. B* **1986**, *34*, 2131–2139. [[CrossRef](#)]
7. Girlando, A.; Painelli, A. Regular-dimerized stack vs neutral-ionic instability in mixed stack CT crystals. *Physica B + C* **1986**, *143*, 559–561. [[CrossRef](#)]
8. Ferrari, E.; Mezzadri, F.; Masino, M. Temperature-induced neutral-to-ionic phase transition of the charge-transfer crystal tetrathiafulvalene-fluoranil. *Phys. Rev. B* **2022**, *105*, 054106. [[CrossRef](#)]
9. Collet, E.; Buron-Le Cointe, M.; Lemée-Cailleau, M.; Cailleau, H.; Toupet, L.; Meven, M.; Mattauch, S.; Heger, G.; Karl, N. Structural evidence of ferroelectric neutral-ionic layered ordering in 2, 6-dimethyltetrathiafulvalene-p-chloranil. *Phys. Rev. B* **2001**, *63*, 054105. [[CrossRef](#)]
10. Ranzieri, P.; Masino, M.; Girlando, A.; Lemée-Cailleau, M.H. Temperature-induced valence and structural instability in DMTTF-CA: Single-crystal Raman and infrared measurements. *Phys. Rev. B* **2007**, *76*, 134115. [[CrossRef](#)]

11. Mao, H.; Xu, J.A.; Bell, P. Calibration of the ruby pressure gauge to 800 kbar under quasi-hydrostatic conditions. *J. Geophys. Res. Solid Earth* **1986**, *91*, 4673–4676. [[CrossRef](#)]
12. Bruker. *APEX III*; Bruker AXS Inc.: Madison, WI, USA, 2019.
13. Sheldrick, G.M. Crystal structure refinement with *SHELXL*. *Acta Crystallogr. Sect. C* **2015**, *71*, 3–8. [[CrossRef](#)] [[PubMed](#)]
14. Mayerle, J.J.; Torrance, J.B.; Crowley, J.I. Mixed-stack complexes of tetrathiafulvalene. The structures of the charge-transfer complexes of TTF with chloranil and fluoranil. *Acta Crystallogr. Sect. B* **1979**, *35*, 2988–2995. [[CrossRef](#)]
15. Delchiaro, F.; Girlando, A.; Painelli, A.; Bandyopadhyay, A.; Pati, S.K.; D’Avino, G. Towards first-principles prediction of valence instabilities in mixed stack charge-transfer crystals. *Phys. Rev. B* **2017**, *95*, 155125. [[CrossRef](#)]
16. Aoki, S.; Nakayama, T.; Miura, A. Temperature-induced neutral-ionic transition in dimethyltetrathiafulvalene-p-chloranil. *Phys. Rev. B* **1993**, *48*, 626. [[CrossRef](#)]
17. Aoki, S.; Nakayama, T.; Miura, A. Neutral-ionic transition in dimethyl-TTF-chloranil. *Synth. Met.* **1995**, *70*, 1243–1244. [[CrossRef](#)]
18. Horiuchi, S.; Okimoto, Y.; Kumai, R.; Tokura, Y. Ferroelectric Valence Transition and Phase Diagram of a Series of Charge-Transfer Complexes of 4,4’-Dimethyltetrathiafulvalene and Tetrahalo-p-benzoquinones. *J. Am. Chem. Soc.* **2001**, *123*, 665–670. [[CrossRef](#)]
19. Sunami, K.; Iwase, F.; Miyagawa, K.; Horiuchi, S.; Kobayashi, K.; Kumai, R.; Kanoda, K. Variation in the nature of the neutral-ionic transition in DM-TTF-QCl 4 under pressure probed by NQR and NMR. *Phys. Rev. B* **2019**, *99*, 125133. [[CrossRef](#)]
20. D’Avino, G.; Masino, M.; Girlando, A.; Painelli, A. Correlated electrons in soft lattices: Raman scattering evidence of the nonequilibrium dielectric divergence at the neutral-ionic phase transition. *Phys. Rev. B* **2011**, *83*, 161105. [[CrossRef](#)]
21. Girlando, A.; Marzola, F.; Pecile, C.; Torrance, J.B. Vibrational spectroscopy of mixed stack organic semiconductors: Neutral and ionic phases of tetrathiafulvalene-chloranil (TTF-CA) charge transfer complex. *J. Chem. Phys.* **1983**, *79*, 1075–1085. [[CrossRef](#)]
22. Kaźmierczak, M.; Patyk-Kaźmierczak, E.; Katrusiak, A. Compression and Thermal Expansion in Organic and Metal–Organic Crystals: The Pressure–Temperature Correspondence Rule. *Cryst. Growth Des.* **2021**, *21*, 2196–2204. [[CrossRef](#)]
23. Girlando, A.; Pecile, C. Vibrational spectra of fluoranil. (2, 3, 5, 6-Tetrafluorop- benzoquinone). *J. Chem. Soc. Faraday Trans.* **1975**, *71*, 689–698. [[CrossRef](#)]
24. Bozio, R.; Zanon, I.; Girlando, A.; Pecile, C. Vibrational spectroscopy of molecular constituents of one-dimensional organic conductors. Tetrathiofulvalene (TTF), TTF+, and (TTF+)2 dimer. *J. Chem. Phys.* **1979**, *71*, 2282–2293. [[CrossRef](#)]

Disclaimer/Publisher’s Note: The statements, opinions and data contained in all publications are solely those of the individual author(s) and contributor(s) and not of MDPI and/or the editor(s). MDPI and/or the editor(s) disclaim responsibility for any injury to people or property resulting from any ideas, methods, instructions or products referred to in the content.